Neutron diffraction structural study of the apatite-type oxide ion conductor, La8Y2Ge6O27

Kendrick, Emma; Orera, Alodia; Slater, Peter

DOI:
10.1039/b911404a

Document Version
Early version, also known as pre-print

Citation for published version (Harvard):
Kendrick, E, Orera, A & Slater, P 2009, 'Neutron diffraction structural study of the apatite-type oxide ion conductor, La8Y2Ge6O27: location of the interstitial oxide ion site', *Journal of Materials Chemistry*, vol. 19, no. 42, pp. 7955-7958. https://doi.org/10.1039/b911404a

Neutron diffraction structural study of the apatite-type oxide ion conductor, $La_8Y_2Ge_6O_{27}$: location of the interstitial oxide ion site

E. Kendrick[1,2], A. Orera[3] and P.R. Slater[3*]

[1]Chemical Sciences, University of Surrey, Guildford, Surrey, GU2 7XH, UK

[2] FiFe batteries, E1 Culham Science Centre, Abingdon, Oxfordshire, OX14 3DB, UK

[3]School of Chemistry, University of Birmingham, Birmingham. B15 2TT. UK

[*]Correspondence to:

Dr. P.R. Slater

School of Chemistry, University of Birmingham, Birmingham. B15 2TT. UK

Tel. +44 (0)121 4148906

Fax +44 (0) 121 414403

p.r.slater@bham.ac.uk

Abstract

Apatite-type rare earth silicates/germanates have attracted considerable interest recently due to their high oxide ion conductivities. Despite evidence in support of a conduction mechanism involving interstitial oxide ions, the exact location of the interstitial oxide ion sites continues to attract controversy. In this paper we report a neutron diffraction structural study for the high oxygen excess compound, $La_8Y_2Ge_6O_{27}$. The structural model indicates that the oxide ions are located between the GeO_4 tetrahedra, leading to significant localised distortions. These results, coupled with recent modelling studies, hence, support the conclusion that oxide ion migration proceeds via these tetrahedra.

1. Introduction

The drive to reduce greenhouse gas emissions, and increase energy efficiency, has driven considerable research into solid oxide fuel cell systems for stationary power applications. This technological interest has fuelled research into new materials for use in such devices, and systems that have attracted significant recent interest in this respect are the apatite-type silicates/germanates, $La_{9.33+x}(Si/GeO_4)_6O_{2+3x/2}$ [1-32]. These silicates/germanates have been shown to exhibit high oxide ion conductivities offering potential use as electrolytes in SOFCs [13]. In contrast to the traditional fluorite and perovskite-type oxide ion conductors, where a conduction mechanism via the presence of oxide ion vacancies has long been universally accepted, the conduction mechanism of the apatite systems has been more controversial. Initial it was assumed that these too were oxide ion vacancy conductors, although there is now an established body of evidence in support of a mechanism involving interstitial oxide ions: these interstitial oxide ions can be either present as oxygen hyperstoichiometry ($x>0$) or Frenkel defects [4, 9, 10, 12, 13, 20-23, 28]. Despite the current acceptance of an interstitial oxide ion conduction mechanism, the location of these interstitial oxide ions and their migration pathway is still somewhat controversial [see review articles [13] and references therein], which can be related to the complex structural features of these apatite systems.

Apatite materials have general formula, $A_{10}(MO_4)_6X_2$ (A=alkaline earth, rare earth, Pb; M=Si, Ge, P, V; X=O, OH, halides), and there are two ways of describing their structure. Traditionally they have been described as comprising of isolated MO_4 tetrahedra arranged so as to form distinct X anion and A cation channels running parallel to the *c* axis. More recently, an alternative description has been proposed, in terms of a "microporous" framework ($A(1)_4(MO_4)_6$) composed of face sharing $A(1)O_6$

trigonal meta-prismatic columns, that are corner connected to the MO_4 tetrahedra. The remaining $A(2)_6X_2$ units occupy the "cavities" within this framework (Figure 1) [20].

As mentioned above, the location of the interstitial oxide ion site in the apatite silicates/germanates has attracted some controversy, with two models for this interstitial site having been proposed: occupancy of a position in the centre of the [0,0,z] channels, situated between O(5) oxygen sites, and occupancy of an interstitial position lying close to the SiO_4/GeO_4 structural units [4, 9-13, 16, 20-23, 27, 28]. This difficulty in conclusively locating the interstitial site can be attributed to the low interstitial oxide ion contents and the considerable local distortions that arise on the introduction of an interstitial oxide ion defect. Nevertheless, there is growing support for the second of these models, initially proposed by atomistic modelling studies, and with a number of supporting experimental reports, including diffraction [10, 16, 20, 21], Mössbauer [11], NMR and Raman studies [12, 23].

An additional structural complexity in the case of the lanthanum germanate apatites, $La_{9.33+z}(GeO_4)_6O_{2+3z/2}$ is the fact that as the La content, and hence oxygen content increases there is a change from a hexagonal to a triclinic cell. Thus Leon-Reina *et al.* have reported the preparation of single phase samples of $La_{9.33+z}(GeO_4)_6O_{2+3z/2}$ for $0.19 \leq z \leq 0.42$, with samples in the range $0.19 \leq z \leq 0.27$ possessing hexagonal symmetry, while samples with higher La content, $0.33 \leq z \leq 0.42$, exhibit a triclinic cell [6]. More recently, Pramana et al. have reported the synthesis of the x=0.67 endmember, which is also triclinic [20]. The triclinic apatites have reduced conductivity at low temperatures, attributed to enhanced defect trapping in this lower symmetry cell, which is a problem in terms of applications. Recently we have shown that Y can be selectively doped into the sites within the $A(1)_4(MO_4)_6$ framework altering the size of

this framework, and hence relieving the triclinic distortion [18]. Thus it is possible through Y doping to prepare hexagonal samples with high oxygen content, i.e. $La_{7.33+x}Y_2(GeO_4)_6O_{2+3x/2}$ ($0 \leq x \leq 0.67$). These samples show enhanced conductivity at low temperatures compared with equivalent triclinic samples without Y doping [18]. In this paper we report neutron diffraction studies of the sample $La_8Y_2(GeO_4)_6O_3$, which has a high interstitial oxide ion content, with a view to confirming the location of the interstitial oxide ion sites.

2. Experimental

Single phase $La_8Y_2(GeO_4)_6O_3$ was prepared via a Pechini-type sol gel route. Stoichiometric amounts of $La(NO_3)_3.6H_2O$, $Y(NO_3)_3.6H_2O$ and GeO_2 were dissolved by heating in water. Once dissolved, citric acid and ethylene glycol were added (1.7 moles per mole of La+Y), and the mixture evaporated on a hot plate until a clear gel was obtained. The gel was then transferred to a furnace and heated at 2°C/min to 800°C before holding at this temperature for 12 hours, followed by regrinding and reheating to 1100°C for a further 12 hours.

Time of flight powder neutron diffraction data were collected at room temperature on the POLARIS diffractometer at the ISIS pulsed spallation source, Rutherford Appleton Laboratory, UK. Data sets from two banks of detectors were used for the refinement; the first was the data from the backscattering (BS) detector bank (average $2\theta \approx 145^{\circ}$) and the second was the data from the 90° detector bank. Structure refinement was then performed using the GSAS suite of Rietveld refinement software [33].

3. Results and Discussion

Space group $P6_3/m$, which is typical for apatite systems, was employed, with Y located on the La1 site in agreement with prior X-ray diffraction studies [18]. The initial structural refinement considered the non-electroneutral cell $La_8Y_2(GeO_4)_6O_2$ containing no interstitial oxide ions, which led to a generally poor fit to the data. Fourier maps showed the presence of unfitted nuclear density between two GeO_4 units, at a position close to (0,0.5,0). In addition, the Fourier maps suggested significant disorder within the oxide-ion sites of the GeO_4 tetrahedra (O1-O3), and the channel oxide ion site (O4). In particular, there was evidence for split sites for the O1 and O3 oxide ions of the GeO_4 tetrahedra, while for the channel oxide ion site, O4, a large spread of nuclear density along z was observed, indicative of static disorder. In order to account for these features, the structural model was refined to include the interstitial site, and split O1, O3, and O4 sites. In order to maintain a stable refinement, the thermal displacement parameters of the split O1 (O1a/O1b) and O3 (O3a/O3b) sites were constrained as equal, while the occupancies were linked such that the total occupancy (O1a+O1b, O3a+O3b) =1.0; for the O4 site, the oxide ion was simply allowed to move off –site along z giving a site with half occupancy. Due to the high correlation between the site occupancy factor and the thermal displacement parameter for the interstitial site, the occupancy was fixed at that expected for the sample stoichiometry. Inclusion of the interstitial oxide-ion sites and split O1, O3, and O4 sites led to a substantial improvement in fit, with good agreement between observed and calculated profiles (figure 2). The final structural model is given in table 1, with selected bond distances in table 2.

The final refined structural model demonstrates the occupancy of interstitial sites (O5) between 2 GeO_4 units. The refined position gives sensible Ge-O distances (table 2),

and is in agreement with recent modelling predictions, and structural studies by Pramana *et al.* for the triclinic apatite $La_{10}(GeO_4)_6O_3$ [20, 21]. In addition to the presence of the interstitial oxide-ion site, there was a need to split the O1 and O3 sites of the GeO_4 tetrahedra to achieve a good fit to the data, with all the split sites again giving sensible bond distances in support of their inclusion.

These observations of the need for split sites emphasise the difficulty in identifying the interstitial oxide-ion sites in these apatite materials through neutron diffraction studies, which essentially give only an average structure. There are two potential origins for the observation of the need to employ split oxide ion sites:

1. Local structural distortions around the interstitial oxide ion.

2. Local distortion around the Y dopant (due to the significantly smaller size of Y compared to La).

In understanding these local distortions, computer modelling studies can provide important detail [17,22]. Our prior computer modelling studies on the oxygen stoichiometric $La_{9.33}(GeO_4)_6O_2$ system have shown that the introduction of an interstitial oxide ion effectively creates a "Ge_2O_9" unit, leading to significant local structural distortions around these Ge atoms [22]. Furthermore, a displacement of the O4 channel oxide ion site is also observed in agreement with the need to allow this oxide ion to move off the ideal site.

It is interesting to note that for both the O1 and O3 sites, the ratio of the two split sites is approximately 2:1, which would be consistent with that expected if we consider the formula as $La_8Y_2(GeO_4)_4(Ge_2O_9)O_2$, and so would add credence to the notion that the occupancy of an interstitial oxide site is the main cause for the need to employ split O1 and O3 sites. Overall the results clearly show that, in any structural model of apatite-type systems, the effect of interstitial oxide-ions on the neighbouring atoms

needs to be considered. It therefore explains the difficulty in obtaining reliable structural refinements of these apatite systems, and also accounts for the high thermal displacement parameters of the oxide-ions associated with the tetrahedra observed in structural studies of other apatite-type oxide ion conductors [4, 10, 17, 19, 28].

With regard to the oxide-ion conducting characteristics of $La_8Y_2(GeO_4)_6O_3$, the location of the interstitial site is important. The refinement shows the presence of interstitial oxide ions between 2 GeO_4 units in adjacent channels, similar to positions observed in the conduction pathway along the *c* direction proposed by the modelling studies (figure 3) [22]. The neutron diffraction studies therefore add support to the modelling studies on $La_{9.33}(GeO_4)_6O_2$ regarding both the interstitial site location, and conduction pathways. These studies predicted that conduction of the interstitial sites occurs along the c direction by a complex fan-like mechanism down the centre of the GeO_4 units (figure 3), while conduction perpendicular to c can occur by the breaking and reforming of the "Ge_2O_9" units, which can allow the transfer of an oxide ion from one channel to the next [22].

4. Conclusions

In summary, structural studies of the hexagonal oxygen hyperstoichiometric apatite germanate system, $La_8Y_2(GeO_4)_6O_3$ have confirmed modelling predictions [22] and neutron diffraction studies of the related triclinic $La_{10}(GeO_4)_6O_3$ [20], that the interstitial oxide ion is associated with the GeO_4 units. Overall the results show that the $A(1)_4(MO_4)_6$ framework is crucial for the accommodation of interstitial oxide ions and hence their conduction in these apatite-type germanates.

Acknowledgements

We would also like to express thanks to EPSRC for funding and ISIS for the provision neutron diffraction beam time. We would also like to thank Ron Smith for his help in the neutron data collection.

References

1. S. Nakayama, H. Aono, Y. Sadaoka, *Chem. Lett.* (1995) 431.

2. S. Nakayama, M. Sakamoto, M. Higuchi, K. Kodaira, *J. Mater. Sci. Lett*. 19 (2000) 91.

3. S. Tao, J.T.S. Irvine, *Mater. Res. Bull.* 36 (2001) 1245.

4. J.E.H. Sansom, D. Richings, P.R. Slater, *Solid State Ionics* 139 (2001) 205.

5. H. Arikawa, H. Nishiguchi, T. Ishihara, Y. Takita, *Solid State Ionics* 136-137 (2000) 31.

6. L. Leon-Reina, M.E. Martin-Sedeno, E.R. Losilla, A. Caberza, M. Martinez-Lara, S. Bruque, F.M.B. Marques, D.V. Sheptvakov, M.A.G. Aranda; *Chem. Mater*. 15 (2003) 2099.

7. E.J. Abram, C.A. Kirk, D.C. Sinclair, A.R. West; *Solid State Ionics* 176 (2005) 1941.

8. J.E.H. Sansom, L. Hildebrandt, P.R. Slater, *Ionics* 8 (2002) 155.

9. J.R. Tolchard, M.S. Islam, P.R. Slater; *J. Mater. Chem.* 13 (2003) 1956; A. Jones, P.R. Slater, M.S. Islam; Chem Mater 20 (2008) 5055.

10. L. Leon-Reina, E.R. Losilla, M. Martinez-Lara, M.C. Martin-Sedeno, S. Bruque, P.Nunez, D.V. Sheptyakov, M.A.G. Aranda; *Chem. Mater*. 17 (2005) 596; L. Leon-

Reina, E.R. Losilla, M. Martinez-Lara, S. Bruque, A. Llobet, D.V. Sheptyakov, M.A.G. Aranda; *J. Mater. Chem.* 15 (2005) 2489.

11. V.V. Kharton, A.L. Shaula, M.V. Patrakeev, J.C. Waerenborgh, D.P. Rojas, N.P. Vyshatko, E.V. Tsipis, A.A. Yaremchenko, F.M.B. Marques; *J. Electrochem. Soc.* 151 (2004) A1236.

12. J.E.H. Sansom, J.R. Tolchard, D. Apperley, M.S. Islam, P.R. Slater; *J. Mater. Chem.* 16 (2006) 1410.

13. E. Kendrick, M.S. Islam, P.R. Slater; *J. Mater. Chem*. 17 (2007) 3104; P.R. Slater, J.E.H. Sansom, J.R. Tolchard; *The Chemical Record* 4 (2004) 373.

14. Y. Masubuchi, M. Higuchi, S. Kikkawa, K. Kodaira, S. Nakayama; *Solid State Ionics* 175 (2004**)** 357.

15. S. Celerier, C. Laberty-Robert, J.W. Long, K.A. Pettigrew, R.M. Stroud, D.R. Rolison, F. Ansart, P. Stevens, *Adv. Mater*. 18 (2006**)** 615.

16. L. Leon-Reina, J.M. Porras-Vasquez, E.R. Losilla, M.A.G. Aranda; *J. Solid State Chem.* 180 (2007) 1250.

17. E. Kendrick, J.R.Tolchard, J.E.H. Sansom, M.S. Islam, P.R. Slater; *Faraday Discussions* 134 (2007) 181.

18. E. Kendrick, P.R. Slater; *Mater. Res. Bull*. 43 (2008) 2509.

19. P. Berastegui, S. Hull, F.J. Garcia Garcia, and J. Grins; *J. Solid State Chem.* 168 (2002) 294.

20. S. S. Pramana, W.T. Klooster and T. J. White; *Acta Cryst*. B 63 (2007) 597.

21. S.S. Pramana, W.T. Klooster, T.J. White; *J. Solid State Chem*. 181 (2008) 1717.

22. E. Kendrick, M.S. Islam, P.R. Slater; *Chem. Commun*. (2008) 715.

23. A. Orera, E. Kendrick, D. C. Apperley, V.M. Orera, P.R. Slater; *Dalton Trans*. (2008) 5296.

24. E. Kendrick, P.R. Slater; *Solid State Ionics* 179 (2008) 981.

25. P.J. Panteix, I. Julien, P. Abelard, D. Bernache-Assolant; *Ceram. Int*. 34 (2008) 1579.

26. T. Iwata, K. Fukuda, E. Bechade, O. Masson, I. Julien, E. Champion, P. Thomas; *Solid State Ionics* 178 (2008) 1523.

27. R. Ali, M. Yashima, Y. Matsushita, H. Yoshioka, K. Okoyama, F. Izumi; *Chem. Mater*. 20 (2008) 5203.

28. J.R. Tolchard, P.R. Slater; *J. Phys. Chem. Solids* 69 (2008) 2433.

29. E. Kendrick, P.R. Slater; *Mater. Res. Bull*. 43 (2008) 3627.

30. E. Kendrick, K.S. Knight, P.R. Slater; *Mater. Res. Bull*. (2009); doi 10.1016/j.materresbull.2009.03.002.

31. J.M. Porras-Vazquez, E.R. Losilla, L. Leon-Reina, D. Marrero-Lopez, M.A.G. Aranda; *J. Am. Ceram. Soc.* 92 (2009) 1062.

32. C. Bonhomme, S. Beaudet-Savignat, T. Chartier, P-M. Geffroy, A-L. Sauvet ; *J. Euro. Ceram. Soc*. 29 (2009) 1781.

33. A.C. Larson, R.B. Von Dreele. *Los Alamos National Laboratory, Report*. No LA-UR-86-748 (1987).

Table 1. Final refined structural parameters for $La_8Y_2(GeO_4)_6O_3$

Atom	Site	x	y	z	Fractional occupancy	100x U/Å^2
Y1/La1	4f	1/3	2/3	0.0012(4)	0.5/0.5	1.82(4)
La2	6h	0.2362(2)	-0.0044(2)	1/4	1.0	1.52(3)
Ge	6h	0.4068(2)	0.3843(2)	1/4	1.0	1.46(3)
O1a	6h	0.3187(3)	0.4961(3)	1/4	0.654(4)	1.29(7)
O1b	6h	0.4386(6)	0.5764(8)	1/4	0.346(4)	1.29(7)
O2	6h	0.6110(3)	0.4659(3)	1/4	1.0	*
O3a	12i	0.2827(5)	0.2316(5)	0.1003(6)	0.354(3)	2.95(5)
O3b	12i	0.3643(4)	0.2592(3)	0.0546(3)	0.646(3)	2.95(5)
O4	4e	0	0	0.203(2)	0.5	*
O5	12i	0.070(2)	0.473(2)	-0.043(3)	0.0833	3.1(5)

*Anisotropic thermal displacement parameters

	U11	U22	U33	U12	U13	U23
O2	1.3(1)	1.4(1)	8.9(2)	0.8(1)	0	0
O4	2.3(2)	2.3(2)	9.8(10)	1.2(1)	0	0

Hexagonal, $P6_3/m$; a =b = 9.9148(1), c= 7.1561(1) Å

R_p=0.0321, R_{wp}=0.0194, χ^2=2.826

Table 2. Selected interatomic distances for $La_8Y_2(GeO_4)_6O_3$.

Bond	Bond Distance/ Å	Bond	Bond Distance/ Å
La1/Y1-O1a [x3]	2.410(3)	La2-O1a	2.870(3)
La1/Y1-O1b [x3]	2.449(5)	La2-O1b	2.768(6)
La1/Y1-O2 [x3]	2.447(3)	La2-O2	2.558(3)
La1/Y1-O3b [x3]	2.736(3)	La2-O3a [x2]	2.399(5)
Ge-O1a	1.720(3)	La2-O3a [x2]	3.003(5)
Ge-O1b	1.768(7)	La2-O3a [x2]	2.545(4)
Ge-O2	1.765(3)	La2-O3b [x2]	2.660(3)
Ge-O3a	1.758(4)	La2-O3b [x2]	2.455(3)
Ge-O3b	1.774(3)	La2-O4 [x2]	2.387(2)
Ge-O5	1.60(2)	La2-O5 [x2]	2.94(2)

Figure Legends

Figure 1. The Apatite structure $A_{10}(MO_4)_6X_2$, in terms of an $A(1)_4(MO_4)_6$ framework composed of face sharing $A(1)O_6$ trigonal meta-prismatic columns, that are corner connected to the MO_4 tetrahedra. The remaining $A(2)_6X_2$ units occupy the "cavities".

Figure 2. Observed, calculated, and difference neutron diffraction profiles for $La_8Y_2(GeO_4)_6O_3$

Figure 3. Oxide-ion conduction pathway along the *c* direction proposed from computer modelling studies of $La_{9.33}(GeO_4)_6O_2$ [22], with the interstitial oxide ion positions for $La_8Y_2(GeO_4)_6O_3$ from neutron diffraction superimposed on top to show a similar location.

Figure 1

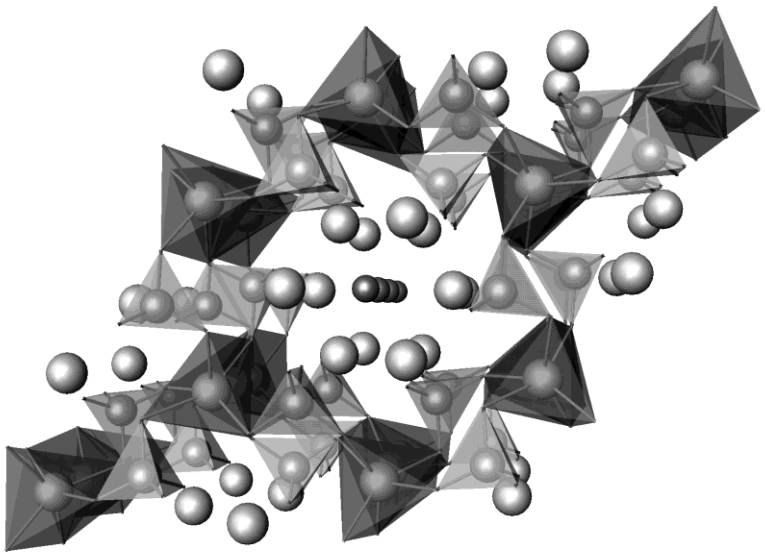

Figure 2.

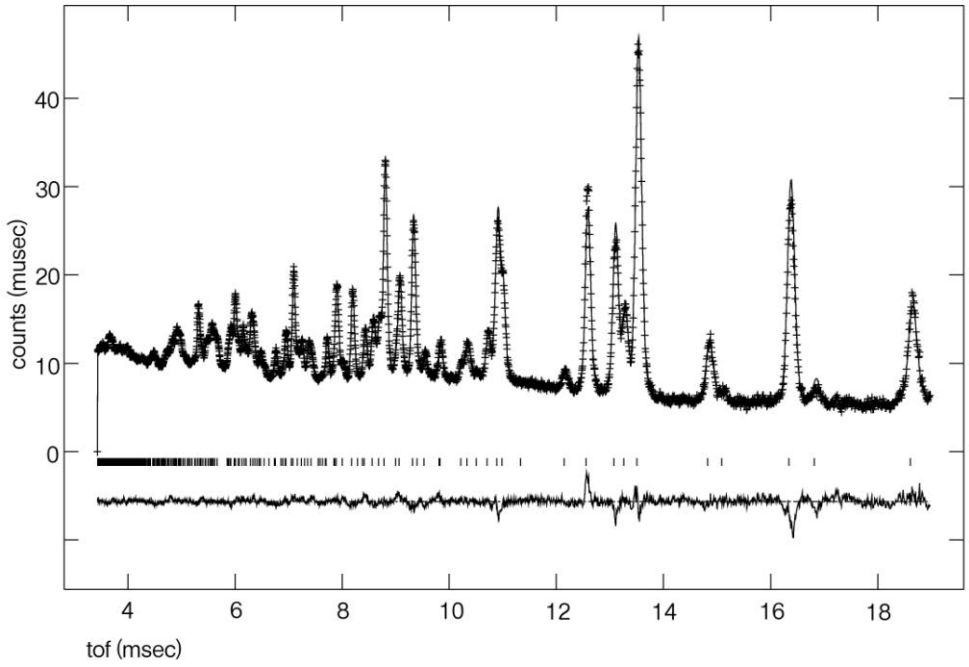

Figure 3.